Journal of Molecular Graphics and Modelling 52 (2014) 82–90

Contents lists available at ScienceDirect

Journal of Molecular Graphics and Modelling

journal homepage: www.elsevier.com/locate/JMGM

Topical Perspectives

Development of a receptor model for efficient *in silico* screening of HIV-1 integrase inhibitors

Mario A. Quevedo[a,*], Sergio R. Ribone[a], Margarita C. Briñón[a], Wim Dehaen[b]

[a] Departamento de Farmacia, Facultad de Ciencias Químicas, Ciudad Universitaria, Universidad Nacional de Córdoba, 5000 Córdoba, Argentina
[b] Molecular Design and Synthesis, Department of Chemistry, KU Leuven, Celestijnenlaan 200F, 3001 Leuven, Belgium

ARTICLE INFO

Article history:
Accepted 20 June 2014
Available online 28 June 2014

Keywords:
Integrase inhibitors
Anti-HIV agents
Molecular docking
Molecular dynamics

ABSTRACT

Integrase (IN) is a key viral enzyme for the replication of the type-1 human immunodeficiency virus (HIV-1), and as such constitutes a relevant therapeutic target for the development of anti-HIV agents. However, the lack of crystallographic data of HIV IN complexed with the corresponding viral DNA has historically hindered the application of modern structure-based drug design techniques to the discovery of new potent IN inhibitors (INIs). Consequently, the development and validation of reliable HIV IN structural models that may be useful for the screening of large databases of chemical compounds is of particular interest. In this study, four HIV-1 IN homology models were evaluated respect to their capability to predict the inhibition potency of a training set comprising 36 previously reported INIs with IC_{50} values in the low nanomolar to the high micromolar range. Also, 9 inactive structurally related compounds were included in this training set. In addition, a crystallographic structure of the IN-DNA complex corresponding to the prototype foamy virus (PFV) was also evaluated as structural model for the screening of inhibitors. The applicability of high throughput screening techniques, such as blind and ligand-guided exhaustive rigid docking was assessed. The receptor models were also refined by molecular dynamics and clustering techniques to assess protein sidechain flexibility and solvent effect on inhibitor binding. Among the studied models, we conclude that the one derived from the X-ray structure of the PFV integrase exhibited the best performance to rank the potencies of the compounds in the training set, with the predictive power being further improved by explicitly modeling five water molecules within the catalytic side of IN. Also, accounting for protein sidechain flexibility enhanced the prediction of inhibition potencies among the studied compounds. Finally, an interaction fingerprint pattern was established for the fast identification of potent IN inhibitors. In conclusion, we report an exhaustively validated receptor model if IN that is useful for the efficient screening of large chemical compounds databases in the search of potent HIV-1 IN inhibitors.

1. Introduction

The life-cycle of type-1 Human Immunodeficiency virus (HIV-1) involves the intervention of multiple enzymes, most of which have been studied as potential molecular targets for the pharmacological treatment of patients suffering from acquired immunodeficiency syndrome (AIDS). Among these enzymes, HIV-1 integrase (IN) was identified early as being a promising therapeutic target [1], since it catalyzes the integration between the viral and host DNA strands, a process that is essential for virus replication and that is not present in human cells, therefore constituting a very selective inhibition mechanism. Unfortunately, the development of IN inhibitors (INIs) has experienced a slow start. Moreover, when compared to other families of anti-HIV drugs, such as the nucleoside reverse transcriptase inhibitors (NRTIs), non-nucleoside reverse transcriptase inhibitors (NNRTIs) and protease inhibitors (PIs), the preclinical and clinical development of INIs has faced greater hurdles [2]. In recent years however, the knowledge gained regarding the molecular mechanisms involved in IN catalytic activity and the way in which this protein interacts with cellular cofactors [3,4], resulted in the development of clinically useful INIs that represented a significant breakthrough in AIDS pharmacotherapeutic protocols [5,6]. These achievements have been further aided by the development of fast and efficient INIs screening assays [7].

The development of INIs initiated with the early identification of molecules containing the β-diketoacid scaffold (**1**, β-DKA, Fig. 1a) and which exhibited inhibitory concentrations (IC_{50}) within the micromolar range [8–10]. Since then, several structure-activity

* Corresponding author. Tel.: +54 351 5353865; fax: +54 351 4334127.
E-mail address: alfredoq@fcq.unc.edu.ar (M.A. Quevedo).

http://dx.doi.org/10.1016/j.jmgm.2014.06.007
1093-3263/

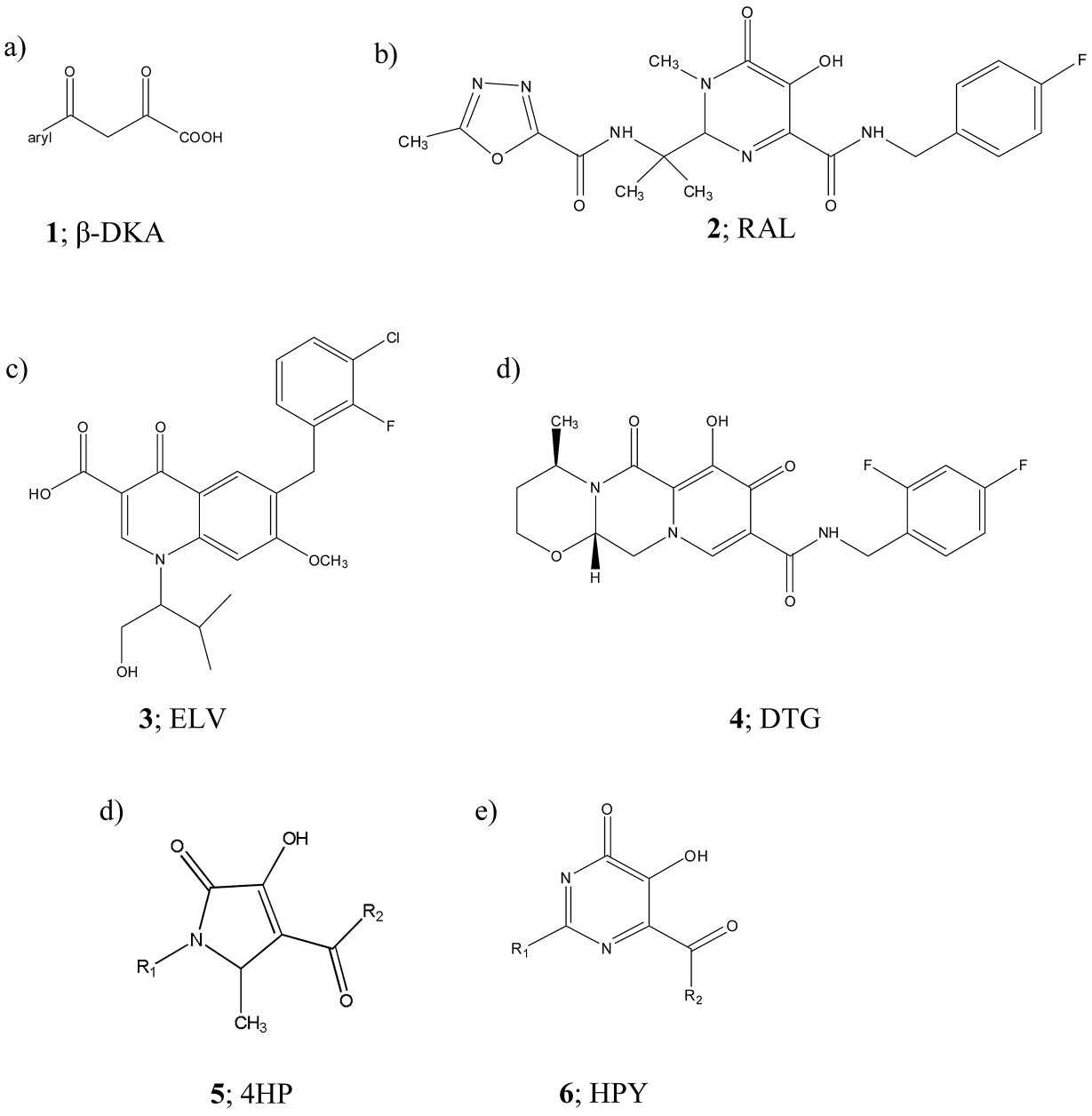

Fig. 1. Chemical structures of the scaffolds and inhibitors with previously reported inhibition activities against HIV-1 IN.

relationships have explored a wide range of β-DKA compounds [9,11,12], with the discovery and approval of raltegravir (**2**, RAL, Fig. 1b) as the first potent and clinically effective IN strand transfer inhibitor [5]. RAL has demonstrated very good pharmacodynamic and pharmacokinetic properties, and although its development constituted a breakthrough for AIDS treatment, its clinical use soon brought about the emergence of resistant viral strains [13,14], evidencing the need to intensify the search of second generation INIs with wider spectrum of activity. Recently, two new INIs have been approved for clinical use in humans, namely elvitegravir (**3**, ELV, Fig. 1c) and dolutegravir (**4**, DTG, Fig. 1d) [15,16]. Also, several promising compounds are in different stages of pre-clinical and clinical development, with intensive efforts toward the search for new inhibitors able to combine enhanced potencies against wild type and mutant strains of IN with adequate biopharmaceutical properties. The need to fulfill these requirements encompasses the exploration of a wide chemical space on INIs structures, suggesting that high throughput virtual screening (vHTS) approaches may represent a very successful search strategy. Computer-aided drug design (CADD) techniques have already contributed significantly to the discovery and optimization of anti-HIV drugs, of which NNRTIs and PIs constitute the landmarks [17–20]. The virtual screening of NNRTIs and PIs was aided by the early obtention of the corresponding molecular targets by X-ray and NMR techniques, allowing the application of ligand (i.e., pharmacophore search, 3D-QSAR) and receptor-based (i.e. molecular docking and molecular dynamics, MD) virtual screening techniques to discover clinically effective compounds [21,22]. On the other hand, the design of INIs has been historically hindered by the lack of experimental structures of full-length IN intasome (i.e. the protein complexed with viral DNA) [4,23–25]. In an attempt to tackle this limitation, several HIV-1 IN intasome homology models have been constructed and further applied to the design of potential INIs [26–31]. Also, the crystal structure of the prototype foamy virus IN (PFV IN) intasome was obtained in complex with the corresponding viral DNA, both in its unbound form and also containing several INIs co-crystallized in

the catalytic site [32,33]. Also the inhibitory activity of RAL and ELV against PFV IN has been previously demonstrated [34], leading to the further suggestion that this model may be useful as a structural template for the vHTS of new INIs [35–37].

Based on the above commented aspects, the present study evaluates the potential of four HIV-1 homology models and one PFV IN X-ray crystal structure as template models useful for the vHTS of INIs. This potential was assessed through evaluation of the ability to predict the inhibitory potencies of a set of 47 previously reported INIs. Also, state of the art techniques to assess protein flexibility and solvent effects on INIs binding to the target models were applied. The reported results are of great utility in the search of new INIs by means of rapid *in silico screening* of chemical compounds databases.

2. Materials and methods

2.1. Integrase (IN) starting structures and models refinements

Starting structures if IN included models obtained both by homology modeling techniques and X-ray diffraction crystallography. Studies on HIV-1 IN were based on four homology models: (a) the one developed by De Luca et al. (*rec1*: pdb code 1WKN) [38,39], (b) the model reported by Wielens et al. (*rec2*: pdb code 1ZA9) [40], (c) the structure deposited by Chen et al. (*rec3*: pdb code 2G3L) [41] and (d) the model recently reported by Johnson et al. (*rec-4*: coordinates kindly provided by the authors) [31]. For HIV-1 IN model refinement procedures, *rec-4* was subjected to explicit molecular MD maintaining explicit crystallographic water molecules. In this way, *rec5* was generated when all water molecules located within the catalytic site were kept explicit as reported by the authors. Also, *rec6* corresponded to the structure in which water molecules inside the catalytic site were modeled based on the crystallographic positions reported in the PFV IN integrase (see model details below). In addition, *rec-7* to *rec-11* corresponded to multiple clustered conformations derived from the molecular dynamics simulations in which the conformational flexibility of explicit solvent molecules and amino acid sidechains were assessed taking as initial structure *rec-5*.

Regarding the PFV IN model, the structure of the IN-DNA-RAL complex reported by Hare et al. (pdb code 3OYA) was used as the starting template [33], with *rec12* and *rec13* corresponding to the structures in which all crystallographic waters were removed and water lying within the catalytic site were kept explicit in their reported positions, respectively. Again, the orientation of explicit water molecules and amino acid sidechains were refined by subjecting *rec13* to MD, with their conformational space being sampled using clustering methods. In this way, the set of receptors *rec14* to *rec18* corresponded to the five clusters of conformations in which only explicit water was allowed reorientation, while *rec19* to *rec23* corresponded to their counterparts in which both explicit water and amino acid sidechains were considered as flexible.

In summary, in this work a total of 23 IN receptors models were evaluated.

2.2. INIs training set (TS)

A TS including 45 molecules was selected in order to evaluate the performance of *rec1–rec23* in predicting the reported inhibition potencies by means of molecular docking. The TS was carefully selected from different reports to fulfill three main criteria; – a wide range of inhibitory potencies (IC_{50}: 2 - >100,000 nM); – consistency among the methods employed for the determination of their biological activity; and – chemical diversity in the pattern of chemical substitutions. In this way, the TS included RAL, ELV and DTG, as well as a series of derivatives structurally related to scaffolds **5** and **6** (Fig. 1d and e), which exhibited diverse chemical modifications (**7–48**, Tables S1-S5), that conferred a wide range of strand transfer inhibitory potencies (IC_{50}, Table S6) [42–46]. Based on the reported IC_{50} values, the TS was subdivided into seven groups: *group-1* corresponded to the most potent compounds with IC_{50} values in the low nanomolar range (IC_{50}: 2–20 nM; $n = 7$), *group-2* included potent inhibitors with IC_{50} in the mid-nanomolar range (IC_{50}: 21–200 nM; $n = 9$), while *group-3* corresponded to moderately potent compounds with IC_{50} within high nanomolar concentration ranges (IC_{50}: 201–1000 nM; $n = 3$). Among less potent compounds, *group-4* included inhibitors exhibiting low micromolar IC_{50} values (1000–30,000 nM; $n = 4$), *group-5* represented compounds with IC_{50} in the mid-micromolar range (IC_{50}: 30,001–60,000 nM; $n = 8$), while *group-6* and *group-7* included very low potency (IC_{50}: 60,001–100,000 nM; $n = 5$) and inactive (IC50: >100,000 nM; $n = 9$) compounds, respectively. According to this information, a potency rank within the TS was assigned (Table S6), which was afterwards used for correlations with molecular docking results.

2.3. Molecular dynamics (MD) simulations

The *Amber12* software package was used to perform MD studies [47]. Ligand atomic charges and molecular parameters were assigned from the restrained electrostatic potential (*RESP*) fitted charges and the *GAFF* force field, respectively [48], while those corresponding to the macromolecule were assigned from the *ff03* force field [49,50]. To carry out model refinement procedures (Section 3.2), MD trajectories were obtained under implicit solvent conditions, in which systems were initially minimized (10,000 steps) and afterwards heated from 0 K to 300 K during 20 ps, using a 2 fs timestep under constant pressure and temperature conditions. The minimized systems were equilibrated for 200 ps, after which the production phase (1 ns) was applied.

When MD runs were performed with the aim of studying the binding energies of selected ligands (Section 3.4), explicit solvent conditions were used, in which a pre-equilibrated TIP3P cubic box of water molecules was constructed and subjected to a two-stage minimization protocol (5000 steps, *phase 1*: solute restrained, *phase 2*: no restraints on the system). The minimized systems were then heated to 300 K (50 ps) with restraints on the solute using a 2 fs timestep. Constant volume conditions were applied, and the SHAKE algorithm was used to constrain bonds involving hydrogen atoms. Heated systems were equilibrated during 100 ps, after which a 2 ns production phase was obtained under constant pressure and temperature conditions.

Clustering over MD trajectories was carried out using the *Cpptraj* module of *Amber12*, while energetic decomposition analyses were performed by applying the Molecular Mechanics Poisson-Boltzmann Surface Area (*MM-PBSA*) approach and visualized using *VMD v.1.9* software [51,52]. Trajectories were obtained using CUDA designed code (*pmemd.cuda*), with computational facilities provided by the GPGPU Computing group at the Facultad de Matemática, Astronomía y Física (FAMAF), Universidad Nacional de Córdoba, Argentina. Intermolecular interactions were detected and depicted using *LigPlot+ v.1.4.4* software [53].

2.4. Molecular docking procedures

Initial ligand structures were constructed using the *PICTO* package developed by OpenEye Scientific Software Inc. [54], and were afterwards subjected to ionization state and tautomer equilibrium analyses considering a pH of 7.0 using the *MoKa* software provided by Molecular Discovery Ltd. [55,56]. The resulting structures were then subjected to conformer analysis using the *OMEGA* software [57,58], applying an energy threshold of 10 kcal/mol, with

the corresponding conformers being assigned *BCC* fitted charges [59] before performing molecular docking runs.

To accomplish docking assays, *rec1-rec23* were processed using the *Fred_Receptor* module developed by OpenEye Scientific Software Inc. [54], in which a cubic box of 10,000 Å^3 was created and centered on both metal cofactors present in the catalytic site. Standard ionization states were assumed for the residues lying within the docking box, with the shape potential grids being calculated as implemented in the software package.

During screening assays, conformer libraries were docked to *rec1-rec23* by applying a fast rigid exhaustive docking method, with a first approach involving the blind docking of the ligands into the binding site using *FRED* software [60,61], while the second one consisted in ligand guided docking as implemented in the *HYBRID* package [62,63]. In this last case, docking poses were filtered based on the position of RAL present in the PFV IN model (pdb: 3OYA). For HIV-1 homology models that did not included a bound inhibitor, RAL positions in the PFV IN was considered for the ligand guided docking procedures.

The resulting docked poses were ranked using the *Chemgauss4* scoring function as implemented in *FRED* and *HYBRID*, selecting the lowest energy binding modes for each ligand, which was further classified according to their docked ranks. To evaluate each model predictive power, plots of the docked rank versus the assigned potency rank were constructed and subjected to statistical analyses using the Origin8 software package. Visualization and analysis of the docked poses were carried out with *VIDA v.4.2.1* software [64].

2.5. Evaluation of model predictive power

To assess quantitatively the power of *rec1-rec23* to predict the inhibitory potencies of the compounds in the TS, the resulting docked ranks were plotted against the corresponding inhibitory potency rank, from which the corresponding correlations were established by linear regression analyses. Six quantitative discriminant criteria were evaluated based on the obtained correlation parameters and defined as follows: (a) *criteria 1* (*C1*): correlation coefficient (r) obtained after inactive compounds were excluded from the linear regression; (b) *criteria 2* (*C2*): number of compounds in *group-1* that were adequately ranked (i.e. within $n = 7$); (c) *criteria 3* (*C3*): number of compounds in *group-1* + *group-2* + *group-3* that were adequately ranked (i.e. within $n = 19$); (d) *criteria 4* (*C4*): number of false positives predictions (i.e. compounds in *group-7* with docked rank < 36); (e) *criteria 5 (C5)*: level at which the first false positive result occurred; (f) *criteria 6* (*C6*): sum of residual squares obtained from the linear regression.

2.6. Application to the virtual screening of a small dataset

In order to further evaluate the predictive power of the receptor models developed, an evaluation training set was constructed from compounds deposited in the ChEMBL database [65]. The training set was constructed by including all compounds bearing the N-(4-fluoropheny)-ethanamide moiety, and that resulted in 5046 molecules with diverse reported biological activities. The downloaded compounds dataset was processed and prepared for docking using KNIME workflows [66], while docking results analyses were performed using Vortex software from Dotmatics [67]. Docking procedures applied were homologous to those described in Section 2.4, using *rec-23* as receptor model. The top 500 hits were extracted and analyzed taking into account their reported biological activity (type and potency). The overall predictive power of *rec-23* was quantitatively assessed by calculating the number of reported IN inhibitors identified within the entire dataset.

3. Results and discussion

3.1. Construction of the TS

The chemical structures corresponding to each reference compound included in the TS are shown in Fig. 1.2–.4 and Tables S1-S5. As can be observed, these molecules share a high structural homology that includes a central ring homologous to the β-DKA scaffold (1, Fig. 1a), feature that constitutes a critical requirement for the coordination of the inhibitor with the metal cofactors present in the binding site. Also, all the compounds included an aromatic ring bound at the C3 and C4 positions (R_2) of 4HP and HPY (**5**–**6**, Fig. 1), a structural feature that has been identified as being critical for the efficient inhibition of the IN catalytic activity [9]. Consequently, the main structural differences among the inhibitors in the selected training set lay in the substitutions introduced in the N1 and C2 positions of **5** and **6** (R_1), and taking into account the wide range of reported potencies for the studied compounds (Table S6), it is evident that intermolecular interactions occurring in this region of the IN binding site had a substantial impact on the resulting antiviral potency.

3.2. Receptor model refinement

In the case of *rec1-rec3*, the structures were used as downloaded from the database and without any further model refinement. Since no information regarding a bound ligand was present, the binding site was assumed to be based on the center of the Mg^{2+} ions located at the catalytic site. Also, *rec1-rec3* contained no information regarding crystallographic water molecules, consequently molecular docking studies were performed solely on the receptor containing the three-dimensional information, as previously reported by the authors of the models [38–41]. In the case of *rec-4*, several refinements over explicit water molecules and amino acid sidechains were performed (details in Section 2.1).

In contrast, the PFV IN crystal structure (pdb code: 3OYA) contained a bound ligand (RAL) and crystallographic waters, which provided useful information for assessing the induced fit effects elicited by the inhibitor on the receptor and solvent. The possibility to evaluate these effects may afford a higher predictive power to the virtual screening of chemical compounds databases, given that rigid docking techniques might be combined with conformational enrichment procedures [68,69]. The downloaded template of IN contained 234 water molecules, of which those located within a 6 Å radii from the ligand were selected and kept explicit, thereby resulting in five additional residues being modeled within the catalytic site (Fig. 2).

These water molecules were identified as *wat1-wat5*, with *wat1-wat3* being coordinated with the two Mg^{2+} ions located within the binding site, while *wat4* was positioned along the interface between RAL and the metal cofactors. The remaining water molecule (*wat5*) was located 6.5 Å away from both Mg^{2+} ions establishing hydrogen bond interactions with the oxadiazole carboxamide moiety of RAL. After performing MD simulations, *wat1-wat5* remained buried in the binding site throughout the trajectory and established stable intermolecular interactions with the surrounding residues, suggesting their structural role in the binding of INIs. No significant displacements from their crystallographic orientations were observed for *wat1-wat3* (Fig. 2). In contrast, *wat4* and *wat5* exhibited significant reorientations within the cavity occupied by the oxadiazole carboxamide moiety of RAL. Figs. S1-S4 presents the intermolecular interactions established between *wat4* and *wat5* with residues lying in the catalytic site, with *wat4* interacting with RAL through hydrogen bonds with the oxygen of the carboxamide functional group (Figures S1.a,c,e, Supplementary Material) and *wat5* interacting with the oxadiazole ring of RAL (Figure S2.b,

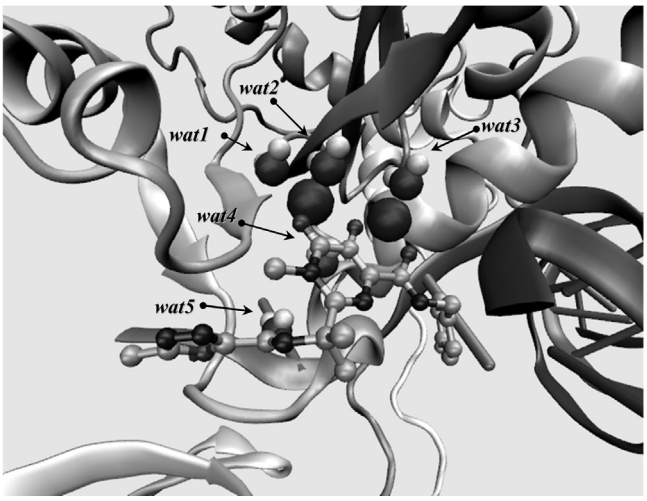

Fig. 2. Positioning of the five crystallographic water molecules (*wat1-wat5*) conserved within the catalytic binding site in pdb 3OYA.

Supplementary Material). When MD optimizations were performed, *wat4* established stable hydrogen bonds with the receptor (Figure S3, Supplementary Material), while *wat5* interacted with the carboxamide moiety of **2** (Figures S4.a,d), demonstrating their structural roles of these solvent molecules.

3.3. Predictive power of receptor models

Molecular docking assays were performed using *rec1-rec23* and the above-mentioned TS, using both a fast rigid exhaustive docking algorithm as well as a ligand guided docking approach [60,62]. From the results obtained, model discrimination powers were evaluated by applying criteria *C1-C6* (for details refer to Section 2.5), with the resulting values being presented in Tables 1 and 2.

As can be seen in entries *1–11*, *24–34* (Tables 1 and 2, respectively), the four homology models of HIV-1 IN presented a lower predictive power than the crystallographic PFV IN receptor model (entries *12–23*, *35–46*, Tables 1 and 2, respectively). The HIV-1 IN models exhibited only poor to mediocre linear correlation coefficient values (*C1* and *C6*). Among them, *rec-4* exhibited the best performance both in blind and ligand guided searches, with acceptable values for *C2*, *C3*, *C4* and *C5* were obtained in both search strategies, indicating a discrimination power toward inhibitors with IC_{50} within the nanomolar range, further supported by its relatively high *C5* value. It is noteworthy that *rec-1*, *rec-2* and *rec-3* exhibited very low *C5* values which confer almost no prediction power to these models, which could not be improved by assessing the effect of explicit solvent molecules or protein sidechain flexibility (Tables 1 and 2).

When results corresponding to *rec12*/*rec23* were analyzed (Tables 1 and 2), higher predictive powers compared to those calculated for *rec-1-rec-11* were found. Also, significant differences among their discrimination criteria values were found, a feature that was highly dependent on the method used for their refinement and the docking approximation implemented (i.e. blind or ligand-based docking). The most powerful receptor model corresponded to *rec23*, particularly when ligand-guided searches were performed (Table 2, entry 46), exhibited the highest level for occurrence of false positive results (*C5* = 28).

Fig. 3a presents the correlation plot between the resulting docked rank and the reported potency rank assigned for each inhibitor in *rec-23* when the HYBRID mode was used. Two outliers can be identified (shown as empty circles), which corresponded to RAL and DLG. These two compounds ranked in a lower position than expected from their inhibition potencies, feature that was further studied by means of MD simulations, as presented later in this work. In addition, Fig. 3b presents the per-residue interaction fingerprint calculated for the whole TS, evidencing that some compounds were not able to interact with the Mg^{2+} cofactors (62 and 71% occupancies for the first and second Mg^{2+} ion, respectively), a key feature for the effective inhibition of IN [70]. In agreement with these reports, all compounds belonging to *group-7* (inactive) did not interact with one or both metal cofactors, while all compounds exhibiting IC_{50} values in the nanomolar range (i.e. *group-1*+*group-2*+*group-3*) were able to coordinate both Mg^{2+} ions, suggesting that the identification of interaction fingerprints constitutes a rapid discrimination criteria in chemical compounds database mining. Also, all compounds in the TS established intermolecular interactions with two nucleotide bases (Nuc1 and Nuc2) of the co-crystallized viral DNA, supporting its critical role in the intasome for the development of a powerful structural model of IN inhibition.

Table 1
Discriminant criteria values obtained using the FRED3 docking algorithm and Chemscore4 scoring function.

Entry: PDB code/*model id.*	*C1**	*C2**	*C3**	*C4**	*C5**	*C6**
1: 1WKN/*rec1*	0.20	3/7	9/19	8	3	3061.36
2: 1ZA9/*rec2*	0.27	1/7	6/19	5	2	2954.82
3: 2G3L/*rec3*	0.07	1/7	7/19	4	1	3179.44
4: rec4	0.50	4/7	13/19	4	18	2385.72
5: rec5	0.29	3/7	11/19	5	10	2927.51
6: rec6	0.33	3/7	12/19	10	11	2846.33
7: rec7	0.42	3/7	11/19	4	11	2840.71
8: rec8	0.20	0/7	7/19	6	3	3061.07
9: rec9	0.27	3/7	12/19	6	6	2954.60
10: *rec10*	0.45	4/7	13/19	6	11	2558.54
11: rec11	0.34	4/7	12/19	4	8	2827.70
12: 3OYA/*rec12*	0.68	4/7	15/19	4	17	1721.19
13: 3OYA/*rec13*	0.65	4/7	15/19	5	20	1809.04
14: 3OYA/*rec14*	0.75	4/7	16/19	5	17	1382.83
15: 3OYA/*rec15*	0.72	5/7	15/19	5	19	1545.63
16: 3OYA/*rec16*	0.71	5/7	15/19	5	17	1561.18
17: 3OYA/*rec17*	0.78	4/7	16/19	5	18	1270.94
18: 3OYA/*rec18*	0.70	5/7	14/19	5	18	1620.65
19: 3OYA/*rec19*	0.59	3/7	14/19	4	4	2068.43
20: 3OYA/*rec20*	0.17	3/7	8/19	5	3	3106.10
21: 3OYA/*rec21*	0.55	4/7	13/19	4	17	2214.47
22: 3OYA/*rec22*	0.51	5/7	10/19	4	10	2549.34
23: 3OYA/*rec23*	0.67	4/7	15/19	5	18	1758.47

Table 2
Discriminant criteria values obtained using the HYBRID docking algorithm and Chemscore4 scoring function.

Entry: PDB code/*model id.*	*C1**	*C2**	*C3**	*C4**	*C5**	*C6**
24: 1WKN/*rec1*	0.43	2/7	12/19	6	7	2614.90
25: 1ZA9/*rec2*	0.17	2/7	10/19	7	8	3103.40
26: 2G3L/*rec3*	0.62	4/7	11/19	7	11	1975.32
27: rec4	0.59	3/7	13/19	4	19	2085.48
28: rec5	0.43	4/7	13/19	6	20	2598.43
29: rec6	0.44	3/7	12/19	4	24	2576.90
30: rec7	0.33	4/7	12/19	4	22	2847.56
31: rec8	0.03	1/7	9/19	4	3	3192.05
32: rec9	0.25	2/7	10/19	5	10	3000.83
33: rec10	0.39	3/7	13/19	5	5	2713.71
34: rec11	0.19	3/7	10/19	3	3	3235.13
35: 3OYA/*rec12*	0.71	4/7	14/19	5	26	1577.63
36: 3OYA/*rec13*	0.70	3/7	15/19	4	23	1609.85
37: 3OYA/*rec14*	0.73	4/7	17/19	6	18	1475.56
38: 3OYA/*rec15*	0.78	3/7	16/19	5	8	1227.43
39: 3OYA/*rec16*	0.70	3/7	15/19	4	25	1616.15
40: 3OYA/*rec17*	0.80	4/7	16/19	4	25	1138.01
41: 3OYA/*rec18*	0.71	4/7	15/19	4	25	1582.20
42: 3OYA/*rec19*	0.69	4/7	14/19	5	23	1665.50
43: 3OYA/*rec20*	0.68	6/7	15/19	4	28	1701.59
44: 3OYA/*rec21*	0.70	4/6	17/19	3	27	1616.25
45: 3OYA/*rec22*	0.69	4/6	17/19	5	26	1680.79
46: 3OYA/*rec23*	0.84	4/7	16/19	4	28	951.16

As part of previous reports, several authors have studied in detail the interaction of RAL, ELV and DTG with key amino acid residues of wild type and mutated HIV IN strains [71,72], with these results being consistent with the interaction fingerprints identified for conserved amino acid residues in PFV IN. In this way, interactions with Asp128, Asp185, Tyr212, Pro214, Gln215 and Glu221 of the PFV IN are homologous to those previously reported for Asp64, Asp116, Tyr143, Pro145, Gln146 and Glu152 in HIV IN. Also, *wat1*, *wat3* and *wat5* established intermolecular interaction with almost all the compounds in the TS.

a)

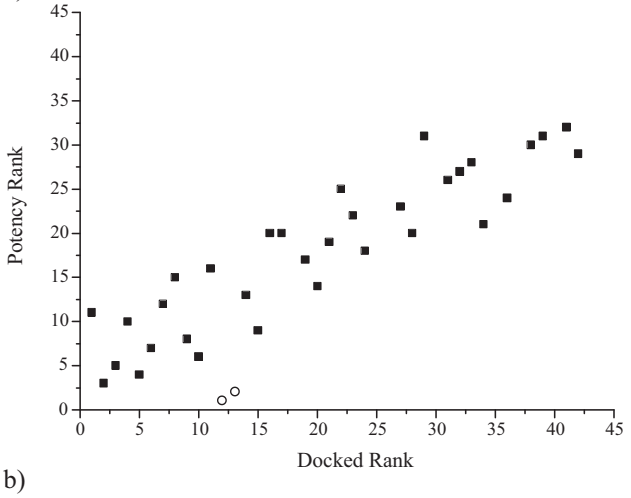

b)

Residue	Occup. %	Residue	Occup. %
Mg2+(1)	62	Glu221	98
Mg2+(2)	71	Gly187	11
Ala188	2	His213	9
Arg329	62	Pro211	15
Asp128	80	Pro214	100
Asp185	93	Tyr212	100
Nuc1	100	Wat1	100
Nuc-2	98	Wat2	40
Nuc3	47	Wat3	100
Gln186	33	Wat4	36
Gln215	80	Wat5	93

Fig. 3. (a) Correlation plots between docked rank and potency rank obtained for the active compounds selected in the training (■) set using *rec23* (inactive compounds were excluded from the analysis). (b) Per-residue interaction fingerprint corresponding the whole set of compounds included in the TS (the binding mode of inactive compounds was included).

3.4. Molecular dynamics (MD) of selected inhibitors

To further study the interaction profiles and the corresponding energetic components between compounds in the TS and *rec-23*, the complexes obtained by molecular docking were further studied by molecular MD. Representative compounds within the TS were selected as follows: all compounds in *group-1* (i.e. RAL, ELV, DTG and **7**–**10**), two low potency compounds (*group-5*: **18**, *group-6*: **26**) and one inactive compound (*group-7*: **37**). Table 3 presents the energetic decomposition analysis obtained for each compound.

When the calculated binding free energy values (i.e. gas phase interaction and total interaction energies) were plotted against the corresponding inhibitory potencies expressed as the pIC50 (Figure S.5.a,b), all compounds in *group-1* exhibited stable interaction components, while low potency and inactive compounds exhibited lower interaction ones. This feature demonstrates that calculation of the binding free energy components constitutes a powerful ranking criterion for the screening of potential INIs. As can be seen in Figure S6, the coordination between RAL and both Mg^{2+} ions is maintained throughout the simulation, originating the strong electrostatic stabilization observed. This behavior was not observed for low potency or inactive compounds originating their low electrostatic interaction components. No significant difference between Van der Waals interaction components was observed among the studied compounds. Although RAL and DTG were not adequately ranked by the rapid screening docking methodology (Fig. 3a), when the energetic components derived from MD are analyzed, both RAL and DTG clearly rank among the most potent compounds (*group-1*), suggesting that their underscoring in the docking runs is originated in biased intermolecular interactions that takes place as a consequence of protein flexibility. In this way, MD followed by energetic decomposition analyses may constitute a powerful complement for the screening of INIs to docking based procedures. However, MD simulations are not practical for the high-throughput screening of chemical compounds databases. Alternatively, additional MD

Table 3
Energetic decomposition analyses performed on the MD trajectories of derivatives of scaffold **4** that exhibited better docking ranks than raltegravir (**2**).

	Cpd.	Elect[a] (kcal/mol)	VdW[b] (kcal/mol)	Gas[c] (kcal/mol)	Pol Solv[d] (kcal/mol)	NP Solv[e] (kcal/mol)	Tot[f] (kcal/mol)
	RAL	−174.6	−39.0	−213.6	170.0	−7.0	−43.6
	ELV	−252.3	−37.9	−290.3	223.2	−6.9	−74.0
	DTG	−150.2	−38.9	−189.1	140.19	−6.4	−55.1
Group-1	7	−194.9	−39.4	−234.3	184.8	−6.3	−55.9
	8	−170.9	−31.6	−202.5	156.6	−6.2	−52.1
	9	−167.2	−37.4	−204.6	158.8	−6.0	−51.9
	10	−145.2	−24.2	−169.4	111.6	−5.3	−57.8
Group-2	18	−0.90	−48.91	−49.8	23.9	−6.8	−32.7
	26	−59.2	−37.3	−96.5	77.6	−6.3	−25.22
Group-3	37	−20.7	−31.2	−51.9	30.8	−4.8	−25.9

and clustering studies dealing with the sampling of the conformational space of IN would be necessary to further enhance the predictive power of *rec-23*. Finally, when compounds belonging to *group-6* and *group-7* were analyzed, very low interaction energies were observed, a feature that was originated in low electrostatic interactions derived from an inefficient coordination with the Mg^{2+} cofactors.

3.5. Virtual screening of an extended dataset

To quantitatively evaluate the screening potential of *rec-23*, a medium-sized molecules dataset including the N-(4-fluoropheny)-ethanamide moiety was constructed and subjected to docking and filtering analyses (see details in Section 2.6). Screened compounds and their corresponding bioactivities were retrieved from the ChEMBL database [65]. The studied dataset contained 5046 molecules with 31882 types of reported bioactivities, among which 1708 (5.35%) corresponded to some kind of anti HIV-1 measurement. After docking procedures were applied using *rec-23*, the top 500 results were selected, of which 420 compounds (84%) corresponded to anti HIV agents. Among them, 364 (87.7%) corresponded to strand transfer inhibitors of HIV-1 IN, which demonstrates an acceptable hit rate of *rec-23*. To further study the discrimination power of *rec-23*, the percent of IN inhibitors detected among the whole dataset (i.e. 5046 molecules) in the top 500 docked results was calculated (Table S.7, Figures S.7). As can be seen, 112 out of 184 compounds (60.9%) exhibiting IC_{50} values below 20 nM were adequately detected. In addition, 259 out of 371 (69.8%) of the compounds exhibiting IC_{50} values below 200 nM were identified, while 70.9% and 70.3% of the IN inhibitors in the 0–1000 and 0–200,000 nM range, respectively, were detected.

4. Conclusions

From the results presented in this work, we conclude that the crystallographic structure of the PFV IN constitutes a powerful model for the high throughput virtual screening of new INIs active against its HIV-1 counterpart. However, to reach adequate screening accuracies, detailed *in silico* methods are required to assess the effect of solvent and protein flexibility in the binding of potential inhibitors. Based on the findings reported and the structural model developed, virtual screening of chemical large compounds databases, such as ZINC [73], appears as a promising strategy for the discovery of new INIs. Also, since crystallographic structures of mutant PFV IN strains are available, an extension of the reported methods for the *in silico* screening of anti HIV-1 agents with broad spectrum of activity merits further exploration.

Acknowledgements

The authors gratefully acknowledge financial support from Secretaría de Ciencia y Técnica of the Universidad Nacional de Córdoba (SECYT-UNC), the Ministerio de Ciencia y Tecnología of Córdoba (MINCyT Córdoba) and the Consejo Nacional de Investigaciones Científicas y Técnicas (CONICET). Mario A. Quevedo acknowledges the GPGPU Computing Group and Dr. Nicolás Wolovick from the Facultad de Matemática, Astronomía y Física (FAMAF), Universidad Nacional de Córdoba, Argentina, for providing access to computing resources. The authors would also like to acknowledge the International Research Offices of KU Leuven and Universidad Nacional de Córdoba for financial support.

Appendix A. Supplementary data

Supplementary data associated with this article can be found, in the online version, at http://dx.doi.org/10.1016/j.jmgm.2014.06.007.

References

[1] A. Engelman, In vivo analysis of retroviral integrase structure and function, Adv. Virus Res. 52 (1999) 411–426.
[2] N. Neamati, HIV-1 integrase inhibitor design: overview and historical perspectives, in: N. Neamati (Ed.), HIV-1 Integrase: Mechanism and Inhibitor Design, Wiley, 2011, pp. 65–196.
[3] A. Ciuffi, M. Llano, E. Poeschla, C. Hoffmann, J. Leipzig, P. Shinn, J.R. Ecker, F. Bushman, A role for LEDGF/p75 in targeting HIV DNA integration, Nat. Med. 11 (12) (2005) 1287–1289.
[4] P. Cherepanov, Integrase illuminated, EMBO Rep. 11 (5) (2010) 328.
[5] V. Summa, A. Petrocchi, F. Bonelli, B. Crescenzi, M. Donghi, M. Ferrara, F. Fiore, C. Gardelli, O.G. Paz, D.J. Hazuda, P. Jones, O. Kinzel, R. Laufer, E. Monteagudo, E. Muraglia, E. Nizi, F. Orvieto, P. Pace, G. Pescatore, R. Scarpelli, K. Stillmock, M.V. Witmer, M. Rowley, Discovery of raltegravir, a potent, selective orally bioavailable HIV-integrase inhibitor for the treatment of HIV-AIDS infection, J. Med. Chem. 51 (18) (2008) 5843–5855.
[6] J.L. Blanco Arévalo, G.G. Whitlock, Dolutegravir: an exciting new kid on the block, Expert Opin. Pharmacother. 15 (4) (2014) 573–582.
[7] J. Demeulemeester, C. Tintori, M. Botta, Z. Debyser, F. Christ, Development of an AlphaScreen-based HIV-1 integrase dimerization assay for discovery of novel allosteric inhibitors, J. Biomol. Screen. 17 (5) (2012) 618–628.
[8] J.S. Wai, M.S. Egbertson, L.S. Payne, T.E. Fisher, M.W. Embrey, L.O. Tran, J.Y. Melamed, H.M. Langford, J.P. Guare Jr., L. Zhuang, V.E. Grey, J.P. Vacca, M.K. Holloway, A.M. Naylor-Olsen, D.J. Hazuda, P.J. Felock, A.L. Wolfe, K.A. Stillmock, W.A. Schleif, L.J. Gabryelski, S.D. Young, 4-Aryl-2,4-dioxobutanoic acid inhibitors of HIV-1 integrase and viral replication in cells, J. Med. Chem. 43 (26) (2000) 4923–4926.
[9] K.D. Beare, M.J. Coster, P.J. Rutledge, Diketoacid inhibitors of HIV-1 integrase: from L-708,906 to raltegravir and beyond, Curr. Med. Chem. 19 (8) (2012) 1177–1192.
[10] D.J. Hazuda, P. Felock, M. Witmer, A. Wolfe, K. Stillmock, J.A. Grobler, A. Espeseth, L. Gabryelski, W. Schleif, C. Blau, M.D. Miller, Inhibitors of strand transfer that prevent integration and inhibit HIV-1 replication in cells, Science 287 (5453) (2000) 646–650.
[11] A. Petrocchi, U. Koch, V.G. Matassa, B. Pacini, K.A. Stillmock, V. Summa, From dihydroxypyrimidine carboxylic acids to carboxamide HIV-1 integrase inhibitors: SAR around the amide moiety, Bioorg. Med. Chem. Lett. 17 (2) (2007) 350–353.
[12] V. Summa, A. Petrocchi, V.G. Matassa, M. Taliani, R. Laufer, R. De Francesco, S. Altamura, P. Pace, HCV NS5b RNA-dependent RNA polymerase inhibitors: From α,(- diketoacids to 4,5-dihydroxypyrimidine- or 3-methyl-5-hydroxypyrimidinonecarboxylic acids. Design and synthesis, J. Med. Chem. 47 (22) (2004) 5336–5339.

[13] C. Charpentier, M. Karmochkine, D. Laureillard, P. Tisserand, L. Bélec, L. Weiss, A. Si-mohamed, C. Piketty, Drug resistance profiles for the HIV integrase gene in patients failing raltegravir salvage therapy, HIV Med. 9 (9) (2008) 765–770.
[14] N. Sichtig, S. Sierra, R. Kaiser, M. Däumer, S. Reuter, E. Schülter, A. Altmann, G. Fätkenheuer, U. Dittmer, H. Pfister, S. Esser, Evolution of raltegravir resistance during therapy, J. Antimicrob. Chemother. 64 (1) (2009) 25–32.
[15] T. Wills, V. Vega, Elvitegravir: a once-daily inhibitor of HIV-1 integrase, Expert Opin Investig Drugs 21 (3) (2012) 395–401.
[16] M.A. Boyd, B. Donovan, Antiretroviral therapy: Dolutegravir sets SAIL(ING), The Lancet 382 (9893) (2013) 664–666.
[17] D. Pandit, S.S. So, H. Sun, Enhancing specificity and sensitivity of pharmacophore-based virtual screening by incorporating chemical and shape features - a case study of HIV protease inhibitors, J. Chem. Inf. Model 46 (3) (2006) 1236–1244.
[18] H.K. Srivastava, G.N. Sastry, Molecular dynamics investigation on a series of HIV protease inhibitors: assessing the performance of MM-PBSA and MM-GBSA approaches, J. Chem. Inf. Model 52 (11) (2012) 3088–3098.
[19] M.L. Barreca, L. De Luca, N. Iraci, A. Rao, S. Ferro, G. Maga, A. Chimirri, Structure-based pharmacophore identification of new chemical scaffolds as non-nucleoside reverse transcriptase inhibitors, J. Chem. Inf. Model 47 (2) (2007) 557–562.
[20] G. Barreiro, C.R.W. Guimarães, I. Tubert-Brohman, T.M. Lyons, J. Tirado-Rives, W.L. Jorgensen, Search for non-nucleoside inhibitors of HIV-1 reverse transcriptase using chemical similarity, molecular docking, and MM-GB/SA scoring, J. Chem. Inf. Model 47 (6) (2007) 2416–2428.
[21] H.C. Castro, N.I.V. Loureiro, M. Pujol-Luz, A.M.T. Souza, M.G. Albuquerque, D.O. Santos, L.M. Cabral, I.C. Frugulhetti, C.R. Rodrigues, HIV-1 reverse transcriptase: a therapeutical target in the spotlight, Curr. Med. Chem. 13 (3) (2006) 313–324.
[22] J.M. Louis, R. Ishima, D.A. Torchia, I.T. Weber, HIV-1 protease: structure, dynamics, and inhibition, in: J. Kuan-Teh (Ed.), Advances in Pharmacology, vol. 55, Academic Press, 2007, pp. 261–298.
[23] M. Jaskolski, J.N. Alexandratos, A. Wlodawer, G. Bujacz, Structural studies of retroviral integrases, in: N. Neamati (Ed.), HIV-1 Integrase: Mechanism and Inhibitor Design, Wiley, 2011, pp. 35–49.
[24] C. Liao, M.C. Nicklaus, Computer tools in the discovery of HIV-1 integrase inhibitors, Future Med. Chem. 2 (7) (2010) 1123–1140.
[25] C.M. Farnet, W.A. Haseltine, Determination of viral proteins present in the human immunodeficiency virus type 1 preintegration complex, J. Virol. 65 (4) (1991) 1910–1915.
[26] C. Liao, M.C. Nicklaus, HIV-1 Integrase-DNA Models, in: N. Neamati (Ed.), HIV-1 Integrase: Mechanism and Inhibitor Design, Wiley, 2011, pp. 429–455.
[27] R. Di Santo, R. Costi, A. Roux, M. Artico, A. Lavecchia, L. Marinelli, E. Novellino, L. Palmisano, M. Andreotti, R. Amici, C.M. Galluzzo, L. Nencioni, A.T. Palamara, Y. Pommier, C. Marchand, Novel bifunctional quinolonyl diketo acid derivatives as HIV-1 integrase inhibitors: design, synthesis, biological activities, and mechanism of action, J. Med. Chem. 49 (6) (2006) 1939–1945.
[28] C. Marchand, A.A. Johnson, R.G. Karki, G.C.G. Pais, X. Zhang, K. Cowansage, T.A. Patel, M.C. Nicklaus, T.R. Burke Jr., Y. Pommier, Metal-dependent inhibition of HIV-1 integrase by β-diketo acids and resistance of the soluble double-mutant (F185 K/C280S), Mol. Pharmacol. 64 (3) (2003) 600–609.
[29] C. Liao, R.G. Karki, C. Marchand, Y. Pommier, M.C. Nicklaus, Virtual screening application of a model of full-length HIV-1 integrase complexed with viral DNA, Bioorg. Med. Chem. Lett. 17 (19) (2007) 5361–5365.
[30] W. Xue, J. Qi, Y. Yang, X. Jin, H. Liu, X. Yao, Understanding the effect of drug-resistant mutations of HIV-1 intasome on raltegravir action through molecular modeling study, Mol. Biosyst. 8 (8) (2012) 2135–2144.
[31] B.C. Johnson, M. Métifiot, A. Ferris, Y. Pommier, S.H. Hughes, A homology model of HIV-1 integrase and analysis of mutations designed to test the model, J. Mol. Biol. 425 (12) (2013) 2133–2146.
[32] S. Hare, S.S. Gupta, E. Valkov, A. Engelman, P. Cherepanov, Retroviral intasome assembly and inhibition of DNA strand transfer, Nature 464 (7286) (2010) 232–236.
[33] S. Hare, A.M. Vos, R.F. Clayton, J.W. Thuring, M.D. Cummings, P. Cherepanov, Molecular mechanisms of retroviral integrase inhibition and the evolution of viral resistance, Proc. Natl. Acad. Sci. U. S. A. 107 (46) (2010) 20057–20062.
[34] E. Valkov, S.S. Gupta, S. Hare, A. Helander, P. Roversi, M. McClure, P. Cherepanov, Functional and structural characterization of the integrase from the prototype foamy virus, Nucleic Acids Res. 37 (1) (2009) 243–255.
[35] B.C. Johnson, M. Métifiot, Y. Pommier, S.H. Hughes, Molecular dynamics approaches estimate the binding energy of HIV-1 integrase inhibitors and correlate with in vitro activity, Antimicrob. Agents Chemother. 56 (1) (2012) 411–419.
[36] S. Hare, S.J. Smith, M. Métifiot, A. Jaxa-Chamiec, Y. Pommier, S.H. Hughes, P. Cherepanov, Structural and functional analyses of the second-generation integrase strand transfer inhibitor dolutegravir (S/GSK1349572), Mol. Pharmacol. 80 (4) (2011) 565–572.
[37] M. Métifiot, K. Maddali, B.C. Johnson, S. Hare, S.J. Smith, X.Z. Zhao, C. Marchand, T.R. Burke, S.H. Hughes, P. Cherepanov, Y. Pommier, Activities, crystal structures, and molecular dynamics of dihydro-1H-isoindole derivatives, inhibitors of HIV-1 integrase, ACS Chem. Biol. 8 (1) (2012) 209–217.
[38] L. De Luca, A. Pedretti, G. Vistoli, M.L. Barreca, L. Villa, P. Monforte, A. Chimirri, Analysis of the full-length integrase-DNA complex by a modified approach for DNA docking, Biochem. Biophys. Res. Commun. 310 (4) (2003) 1083–1088.
[39] L. De Luca, G. Vistoli, A. Pedretti, M.L. Barreca, A. Chimirri, Molecular dynamics studies of the full-length integrase-DNA complex, Biochem. Biophys. Res. Commun. 336 (4) (2005) 1010–1016.
[40] J. Wielens, I.T. Crosby, D.K. Chalmers, A three-dimensional model of the human immunodeficiency virus type 1 integration complex, J. Comput. Aided Mol. Des. 19 (5) (2005) 301–317.
[41] A. Chen, I.T. Weber, R.W. Harrison, J. Leis, Identification of amino acids in HIV-1 and avian sarcoma virus integrase subsites required for specific recognition of the long terminal repeat ends, J. Biol. Chem. 281 (7) (2006) 4173–4182.
[42] P. Pace, S.A.H. Spieser, V. Summa, 4-hydroxy-5-pyrrolinone-3-carboxamide HIV-1 integrase inhibitors, Bioorg. Med. Chem. Lett. 18 (14) (2008) 3865–3869.
[43] P. Pace, M.E. Di Francesco, C. Gardelli, S. Harper, E. Muraglia, E. Nizi, F. Orvieto, A. Petrocchi, M. Poma, M. Rowley, R. Scarpelli, R. Laufer, O.G. Paz, E. Monteagudo, F. Bonelli, D. Hazuda, K.A. Stillmock, V. Summa, Dihydroxypyrimidine-4-carboxamides as novel potent and selective HIV integrase inhibitors, J. Med. Chem. 50 (9) (2007) 2225–2239.
[44] R. Dayam, L.Q. Al-Mawsawi, N. Neamati, Substituted 2-pyrrolinone inhibitors of HIV-1 integrase, Bioorg. Med. Chem. Lett. 17 (22) (2007) 6155–6159.
[45] K. Ma, P. Wang, W. Fu, X. Wan, L. Zhou, Y. Chu, D. Ye, Rational design of 2-pyrrolinones as inhibitors of HIV-1 integrase, Bioorg. Med. Chem. Lett. 21 (22) (2011) 6724–6727.
[46] C. Gardelli, E. Nizi, E. Muraglia, B. Crescenzi, M. Ferrara, F. Orvieto, P. Pace, G. Pescatore, M. Poma, M.D.R.R. Ferreira, R. Scarpelli, C.F. Homnick, N. Ikemoto, A. Alfieri, M. Verdirame, F. Bonelli, O.G. Paz, M. Taliani, E. Monteagudo, S. Pesci, R. Laufer, P. Felock, K.A. Stillmock, D. Hazuda, M. Rowley, V. Summa, Discovery and synthesis of HIV integrase inhibitors: development of potent and orally bioavailable N-methyl pyrimidones, J. Med. Chem. 50 (20) (2007) 4953–4975.
[47] D.A. Case, T.E. Cheatham Iii, T. Darden, H. Gohlke, R. Luo, K.M. Merz Jr., A. Onufriev, C. Simmerling, B. Wang, R.J. Woods, The Amber biomolecular simulation programs, J. Comput. Chem. 26 (16) (2005) 1668–1688.
[48] J. Wang, R.M. Wolf, J.W. Caldwell, P.A. Kollman, D.A. Case, Development and testing of a general Amber force field, J. Comput. Chem. 25 (9) (2004) 1157–1174.
[49] Y. Duan, C. Wu, S. Chowdhury, M.C. Lee, G. Xiong, W. Zhang, R. Yang, P. Cieplak, R. Luo, T. Lee, J. Caldwell, J. Wang, P. Kollman, A point-charge force field for molecular mechanics simulations of proteins based on condensed-phase quantum mechanical calculations, J. Comput. Chem. 24 (16) (2003) 1999–2012.
[50] M.C. Lee, Y. Duan, Distinguish protein decoys by using a scoring function based on a new AMBER force field, short molecular dynamics simulations, and the generalized born solvent model, Proteins 55 (3) (2004) 620–634.
[51] B. Kuhn, P. Gerber, T. Schulz-Gasch, M. Stahl, Validation and use of the MM-PBSA approach for drug discovery, J. Med. Chem. 48 (12) (2005) 4040–4048.
[52] W. Humphrey, A. Dalke, K. Schulten, VMD: visual molecular dynamics, J. Mol. Graph. 14 (1) (1996) 33–38.
[53] R.A. Laskowski, M.B. Swindells, LigPlot+: multiple ligand–protein interaction diagrams for drug discovery, J. Chem. Inf. Model 51 (10) (2011) 2778–2786.
[54] OpenEye.Scientific.Software. http://www.eyesopen.com/
[55] F. Milletti, L. Storchi, G. Sforna, G. Cruciani, New and original pKa prediction method using grid molecular interaction fields, J. Chem. Inf. Model 47 (6) (2007) 2172–2181.
[56] F. Milletti, L. Storchi, G. Sfoma, S. Cross, G. Cruciani, Tautomer enumeration and stability prediction for virtual screening on large chemical databases, J. Chem. Inf. Model 49 (1) (2009) 68–75.
[57] Omega.2.4.3. OpenEye Scientific Software, Santa Fe, NM, http://www.eyesopen.com/
[58] P.C.D. Hawkins, A.G. Skillman, G.L. Warren, B.A. Ellingson, M.T. Stahl, Conformer generation with OMEGA: Algorithm and validation using high quality structures from the protein databank and Cambridge structural database, J. Chem. Inf. Model 50 (4) (2010) 572–584.
[59] A. Jakalian, B.L. Bush, D.B. Jack, C.I. Bayly, Fast, efficient generation of high-quality atomic charges. AM1-BCC Model: I. Method, J. Comput. Chem. 21 (2) (2000) 132–146.
[60] M. McGann, FRED pose prediction and virtual screening accuracy, J. Chem. Inf. Model 51 (3) (2011) 578–596.
[61] Fred.3.0.0 OpenEye Scientific Software SF, NM, http://www.eyesopen.com/
[62] M. McGann, FRED and HYBRID docking performance on standardized datasets, J. Comput. Aided Mol. Des. 8 (26) (2012) 1–10.
[63] Hybrid OpenEye Scientific Software, Santa Fe, NM, http://www.eyesopen.com/
[64] VIDA.4.2.1. OpenEye Scientific Software, Santa Fe, NM, http://www.eyesopen.com/
[65] A. Gaulton, L.J. Bellis, A.P. Bento, J. Chambers, M. Davies, A. Hersey, Y. Light, S. McGlinchey, D. Michalovich, B. Al-Lazikani, J.P. Overington, ChEMBL: A large-scale bioactivity database for drug discovery, Nucleic Acids Res. 40 (D1) (2012) D1100–D1107.
[66] M.R. Berthold, N. Cebron, F. Dill, T.R. Gabriel, T. Kötter, T. Meinl, P. Ohl, C. Sieb, K. Thiel, B. Wiswedel, KNIME. The Konstanz information miner, in: Studies in Classification, Data Analysis and Knowledge Organization, 2008, pp. 319–326.
[67] Vortex v2009.04 - http://www.dotmatics.com/
[68] J.A. McCammon, Target flexibility in molecular recognition, Biochim. Biophys. Acta - Proteins Proteomics 1754 (1–2) (2005) 221–224.
[69] S.E. Nichols, R. Baron, A. Ivetac, J.A. McCammon, Predictive power of molecular dynamics receptor structures in virtual screening, J. Chem. Inf. Model 51 (6) (2011) 1439–1446.

[70] A. Bacchi, M. Carcelli, C. Compari, E. Fisicaro, N. Pala, G. Rispoli, D. Rogolino, T.W. Sanchez, M. Sechi, N. Neamati, HIV-1 in strand transfer chelating inhibitors: a focus on metal binding, Mol. Pharm. 8 (2) (2011) 507–519.
[71] W. Xue, X. Jin, L. Ning, M. Wang, H. Liu, X. Yao, Exploring the molecular mechanism of cross-resistance to HIV-1 integrase strand transfer inhibitors by molecular dynamics simulation and residue interaction network analysis, J. Chem. Inf. Model 53 (1) (2013) 210–222.
[72] T. Balaraju, A. Kumar, C. Bal, D. Chattopadhyay, N. Jena, N.C. Bal, A. Sharon, Aromatic interaction profile to understand the molecular basis of raltegravir resistance, Struct. Chem. 24 (5) (2013) 1499–1512.
[73] J.J. Irwin, B.K. Shoichet, ZINC - A free database of commercially available compounds for virtual screening, J. Chem. Inf. Model 45 (1) (2005) 177–182.